Boletim da Sociedade Astronômica Brasileira, **36**, no. 1, 212-215

Evaluating the weak lensing mass bias in the dissociative galaxy cluster Abell 56

Richards P. Albuquerque[1], Rubens E. G. Machado[1], Rogério Monteiro-Oliveira[2]

[1] Universidade Tecnológica Federal do Paraná, Paraná, Brasil. e-mail: richards_pereira12@hotmail.com
[2] Academia Sinica Institute of Astronomy and Astrophysics, Taiwan. e-mail: rogerionline@gmail.com

Abstract. It has been demonstrated that masses derived from weak gravitational lensing during the formation phase of a galaxy cluster may be overestimated due to assuming a regular mass profile to fit the data. This discrepancy can directly influence the outcomes of tailored hydrodynamical simulations based on such biased masses. However, the magnitude of this impact remains unknown, potentially raising questions about the validity of previous efforts to unveil the cluster merger history through these simulations. We addressed this question with the merging cluster Abell 56 as a backdrop, which exhibits evidence of a dissociative bullet-like merger with a likely high inclination angle between the plane of orbit and the sky. Following a dedicated hydrodynamical *N*-body simulation, we identified an optimal model corresponding to a collision that occurred 0.52 Gyr ago, accurately reproducing the observational features of Abell 56, with an inclination of 58°. These features include a 103 kpc offset between the gas density peak and the southern dark matter density peak, gas morphology, a line-of-sight relative velocity of 184 km s^{-1}, and a mean temperature of 6.7 keV. We conclude that the weak lensing mass bias did not significantly impact the recovered dynamics of Abell 56.

Resumo. Foi demonstrado que as massas derivadas por meio de lentes gravitacionais fracas durante a fase de formação de um aglomerado de galáxias podem ser superestimadas devido à suposição de um perfil de massa regular para ajustar os dados. Essa discrepância pode influenciar diretamente os resultados de simulações hidrodinâmicas dedicadas baseadas em tais massas enviesadas. No entanto, a magnitude desse impacto permanece desconhecida, o que pode levantar questionamentos sobre a validade de esforços anteriores para revelar a história de fusão dos aglomerados por meio dessas simulações. Abordamos essa questão utilizando o aglomerado em fusão Abell 56 como cenário, que apresenta evidências de uma fusão dissociativa do tipo 'bullet' com um provável alto ângulo de inclinação entre o plano orbital e o plano do céu. A partir de uma simulação hidrodinâmica de *N*-corpos, identificamos um modelo ótimo correspondente a uma colisão que ocorreu há 0.52 Gyr, reproduzindo as características observacionais do Abell 56 e apresentando uma inclinação de 58°. Essas características incluem um deslocamento de 103 kpc entre o pico de densidade de gás e o pico de densidade de matéria escura no sul, a morfologia do gás, uma velocidade relativa na linha de visada de 184 km s^{-1} e temperatura média de 6.7 keV. Neste cenário, concluímos que o viés de massa proveniente de lentes fracas não teve um impacto significativo na recuperação da dinâmica de Abell 56.

Keywords. Galaxies: clusters: individual: Abell 56 – Gravitational lensing: weak – Methods: numerical

1. Introduction

In the scenario of the standard cosmological model Lambda Cold Dark Matter (ΛCDM), small fluctuations in the initial density field, of the early Universe, were amplified by gravitational force, leading to the collapse of dark matter halos going from a linear to a nonlinear regime (Molnar 2016). Following the hierarchical structure formation paradigm, mergers with substructures of similar sizes and smooth accretions of smaller ones lead to the formation of galaxy clusters (Kravtsov 2012). Clusters are one of the most recent structures to collapse at low redshifts (z). These galaxy clusters are found at the intersections of filamentary structures in the cosmic web. Cosmological simulations are frequently employed to investigate these structures of our Universe (e.g., Nelson 2019).

Galaxy clusters are massive structures whose total mass can exceed 10^{15} $M_\odot$ (e.g., Jauzac 2018). In these environments, spacetime is significantly warped, causing the deflection of light from background galaxies. These effects can be described and quantified through gravitational lensing theory. When a background galaxy is closely aligned with a galaxy cluster along our line of sight, the lensing effect is amplified, resulting in the so-called strong lensing effect. On the other hand, when there is no alignment, the light deflection becomes smoother, leading to the phenomenon known as weak lensing.

The mass of a galaxy cluster is a fundamental parameter for probing theoretical models of large-scale structure formation and evolution, as well as for constraining cosmological parameters (e.g., Kravtsov 2012; Pratt 2019). Among the available methods, weak lensing is the most direct probe of the mass distribution in the Universe. Determining this mass becomes particularly challenging during extreme events, such as mergers, when clusters are significantly perturbed from their equilibrium state. In such scenarios, weak gravitational lensing proves to be a valuable tool for estimating cluster masses, as it does not rely on assumptions of dynamical equilibrium.

However, a significant limitation persists. Estimating cluster mass often relies on the assumption that the halo conforms to an analytical profile, such as the Navarro–Frenk–White (NFW) model (Navarro 1996), along with a mass-concentration relation (e.g., Duffy 2008; Dutton 2014; Diemer 2019). These models are frequently designed to characterize the average properties of halos (Jing 2000). As a result, applying these approaches to individual clusters especially in merging scenarios can introduce systematic errors, complicating the mass determination process.

In a first-order approximation, the weak lensing mass bias is influenced by variations in the cluster concentration parameter. In extreme scenarios such as major mergers, i.e.,where the mass ratio between the two most massive clusters is less than two, the weak lensing mass bias can overestimate cluster masses by up

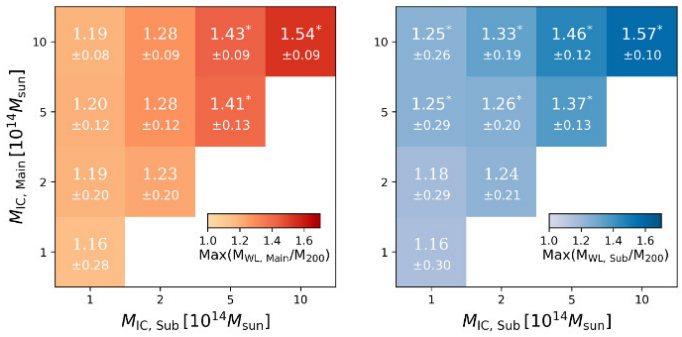

Figure 1. Maximum weak lensing mass bias, with the color gradient indicating the maximum $M_{\rm WL}/M_{200}$. The axes represent the initial masses of the main and sub-clusters. Figure from Lee (2023).

to 60% (Lee 2023). This indicates that the masses reported in existing literature may deviate significantly from the true values.

To investigate the impact of the weak lensing mass bias, Lee (2023) conducted an extensive study. They utilized outputs from hydrodynamic N-body simulations of binary galaxy cluster collisions to create mock weak lensing catalogs that mimic the source galaxy properties observed in real telescope data. The weak lensing ellipticity catalogs were generated at refined time steps, based on the projected mass distribution of the simulated mergers, and halo masses were estimated by simultaneously fitting two NFW profiles.

By comparing the masses directly obtained from the simulation with those derived from the mock weak lensing, it was found that weak lensing can overestimate galaxy cluster masses, depending on the merger stage. The maximum values of the weak lensing mass bias across different merger stages are presented in Figure 1.

Recently, Abell 56 became the focus of a detailed investigation into its mass distribution, revealing evidence of dissociation. While analyzing the $\sim 10,000\,\mathrm{deg}^2$ field of the Sloan Digital Sky Survey, two BCG candidates were identified, separated by a relatively large angular distance of $2'$. After confirming this angular separation, the X-ray peak position was examined and compared to the BCG positions, revealing an offset (Wittman 2023).

The mass of Abell 56 was estimated using the weak lensing technique. In this proceeding, we aim to evaluate the weak lensing mass bias of Abell 56 through hydrodynamic N-body simulations. This work is a continuation of a previous paper Albuquerque (2024), the structure of this proceeding is as follows: in Section 2, we describe the simulation setup. In Section 3, we present the results of the collision scenario, analyze the evolution of the concentration parameter, and apply the weak lensing mass bias correction to investigate its impact on gas morphology and mean temperature. Finally, a summary and the main conclusions are provided in Section 4. In this work, we assumed a standard ΛCDM cosmology model with $\Omega_\Lambda = 0.70$, $\Omega_{\rm M} = 0.30$ and $H_0 = 70\,\mathrm{km\,s^{-1}\,Mpc^{-1}}$.

2. Methods

Investigating the weak lensing mass bias requires sophisticated methods that account for both gravitational forces and gas hydrodynamics. In this work, we performed simulations using the GADGET-4 code (Springel 2021), which implements smoothed particle hydrodynamics (SPH) for gas particles. Our initial conditions were generated with the CLUSTEP code (see Ruggiero (2017).

For our initial conditions, we assumed that the dark matter particles follow the Hernquist (1990) density profile:

$$\rho_{\rm h}(r) = \frac{M_{\rm h}}{2\pi}\frac{a_{\rm h}}{r(r+a_{\rm h})^3}\,, \tag{1}$$

where $M_{\rm h}$ is the total dark matter mass, and a_h is the scale length. For the gas, we adopted the Dehnen (1993) density profile:

$$\rho_{\rm g}(r) = \frac{(3-\gamma)M_{\rm g}}{4\pi}\frac{a_{\rm g}}{r^{\gamma}(r+a_{\rm g})^{4-\gamma}}\,, \tag{2}$$

where $M_{\rm g}$ and $a_{\rm g}$ represent the total gas mass and scale length, respectively. In all simulations, we set $\gamma = 0$, which corresponds to a non-cool core cluster, and baryon fraction of $f_{\rm gas} = 0.1$, consistent with observed clusters in this mass range (Lagana 2013).

For the main cluster the estimated mass was $M_{200} = (4.5 \pm 0.8)\times10^{14}\,\mathrm{M}_\odot$ and for the secondary cluster $M_{200} = (2.8\pm0.7)\times 10^{14}\,\mathrm{M}_\odot$ (Wittman 2023). The total particles number in this simulation was $\sim 10^6$ for both dark matter and gas.

The concentration parameter c is related with the mass and redshift through the Duffy (2008) relation.

$$c = \frac{6.71}{(1+z)^{0.44}}\left(\frac{M_{200}}{2\times10^{12}h^{-1}M_\odot}\right)^{-0.091}\,. \tag{3}$$

From mass concentration relation, we obtain a concentration of $c = 3.8$ and $c = 3.9$ for the main and sub galaxy subclusters, respectively. Using the definition, the concentration parameter is related with radius of the cluster r_{200} and the scale length of the NFW:

$$c \equiv r_{200}/r_{\rm s}\,. \tag{4}$$

This concentration parameter can be utilized to estimate the scale length of the Hernquist density profile

$$a_{\rm h} = r_{\rm s}\sqrt{2[\ln(1+c) - c(1+c)]}\,. \tag{5}$$

We obtained for the sub cluster $a_{\rm h} = 521\,\mathrm{kpc}$ and for the main cluster $a_{\rm h} = 434\,\mathrm{kpc}$.

In the joiner process of the initial condictions, the clusters were separated by 3 Mpc, with an initial approach velocity of $v = 600\,\mathrm{km\,s^{-1}}$ and impact parameters of $b = 200\,\mathrm{kpc}$.

3. Results

After testing various configurations for the collision scenario, we identified a configuration, referred to as the 'early model', that accurately reproduces both the position of the dark matter peak and the main peak of the gas density. Observational data indicates a dark matter peak separation of 438 ± 206 kpc, while our simulations 420 kpc. The gas density peak offset is observed to be 118 ± 41 kpc, while our simulations produce an offset of 132 kpc. The line of sight relative velocity from the observation is $\Delta v = 153\pm281\,\mathrm{km\,s^{-1}}$ and the early scenario is in the plane of the sky, therefore $\Delta v = 0\,\mathrm{km\,s^{-1}}$. In Fig. 2, we present four different stages of the simulations, with the last frame representing the early model, occurring 0.12 Gyr after the pericentric passage.

The temperature within a circular region with a radius of 398 kpc centered on the cluster is approximately $T_X = 5.9^{+1.1}_{-0.8}$ keV. In the early model, we obtained a mean temperature of 9.7 keV. This value significantly exceeds the observational results, well beyond the error bars, prompting us to explore methods to mitigate this higher temperature.

Figure 2. Time evolution of the gas density during the merger scenario, with contour lines representing the dark matter density and the red cross indicating the peak of the gas density. TSC (time since collision) refers to the time elapsed since the pericentric passage. This figure is adapted from Albuquerque (2024).

Figure 3. We depict the time evolution of the concentration parameter normalized to its initial value. The red and blue lines represent the main and sub subclusters, respectively. This figure is adapted from Albuquerque (2024).

The results of Lee (2023) indicate that the difference between the weak lensing and current mass can reach $\sim 60\%$ in merging clusters. This mass overestimation from the weak lensing analysis is attributed, in first order of approximation, to the contraction parameter of the halo. Peaks in the concentration parameter indicates maximum weak lensing mass bias.

The instant attributed to the early model corresponds exactly to the moment when the concentration reaches its maximum, as shown in Fig. 3, suggesting a potential bias. Through scaling relations, the mean temperature and cluster mass are correlated. To mitigate this bias, we applied a weak lensing mass correction. Based on the expected bias values, we found that the mass of the main cluster may be overestimated by $28 \pm 12\%$, while that of the sub cluster may be overestimated by $26 \pm 20\%$, as illustrated in Fig. 1.

Consequently, we reran a new simulation of the early model incorporating the mass correction. This adjustment resulted in new masses of $3.5 \times 10^{14}\,M\odot$ for the main cluster and $2.2 \times 10^{14}\,M\odot$ for the secondary cluster. The resulting temperature map is shown in Fig. 4, with the corrected mass model depicted in the right panel. We obtained a mean temperatures of 9.7 keV for the early scenario and 8.4 keV for the corrected one. The temperature significantly decreased for about 1.3 keV, however it continued exceeding the observational estimation well beyond the error bar.

Regarding the density map, no significant changes were noted. Both models successfully reproduced the main gas peak, as expected from the observational data. However, we were compelled to explore alternative solutions to mitigate the excessively high mean temperature.

We identified a late scenario with a large inclination angle that achieved the expected projected distance between the dark matter peaks. In this model, the system is only 30 kpc short of the apocenter, with a three-dimensional separation of 790 kpc. By inclining the system at an angle of 58° in the plane of the sky, the projected distance between the dark matter peaks was 103 kpc. With a line-of-sight velocity of $\Delta v = 184\,\mathrm{km\,s^{-1}}$ and a mean temperature of 6.7 keV, the late scenario satisfied all the main observational constraints, including achieving an acceptable mean temperature. For further details, see Albuquerque (2024).

4. Conclusions

A56 is a binary galaxy cluster that experienced a dissociative merger. Using idealized simulation, we replicate some observed features and trace its evolutionary history. To achieve this, we tested two scenarios with different masses to match the gas morphology, the observationally constrained distances, and the mean temperature. The projected separation between the dark matter density peaks is 438 ± 206 kpc, the distance between the southern cluster and the main gas density peak is 118 ± 41 kpc, and the line-of-sight relative velocity is $\Delta v = 153 \pm 281\,\mathrm{km\,s^{-1}}$ (Wittman 2023).

Figure 4. Comparison of the temperature maps for the early scenario (upper) and late scenario (lower), with the initial mass derived from weak lensing analyses (a) and the bias-corrected mass (b). The contour lines indicate the dark matter density, with the green circle highlighting the region of interest with $r = 398$ kpc and mean temperatures of 9.7 keV (top) and 6.7 keV (bottom) in column (a), and 8.4 keV (top) and 6.4 keV (bottom) in column (b). Figure from Albuquerque (2024).

The early scenario, at $TSC = 0.12$ Gyr, satisfies key observational constraints, including a well-defined gas density peak near the main cluster and the separation between the dark matter density peaks. However, the mean temperature of 9.7 keV is notably higher than the observed value.

The model with mass correction reproduced the gas and dark matter density peaks at the expected positions, as well as the line-of-sight relative velocity. However, even with the mass correction, the temperature remained excessively high. This suggests that, in the specific configuration of the Abell 56 merger, the weak lensing mass bias correction did not significantly influence the collision dynamics.

The late scenario, at $TSC = 0.52$ Gyr, successfully reproduced the observational constraints for the distances between the dark matter and gas peaks. With a well-defined gas density peak, a mean temperature of 6.7 keV, and a line-of-sight velocity of $\Delta v = 184\,\mathrm{km\,s^{-1}}$, this model aligns well with the observational constraints of Abell 56.

Although our results suggest that the weak lensing mass bias correction does not significantly affect the interpretation of the cluster's merger history, it is too early to consider this a universally applicable conclusion. In certain cluster mergers, the weak lensing mass correction can be fundamental. Further studies involving diverse configurations, especially those examining varying mass ratios and merger stages, are essential to more reliably determine the true impact of the weak lensing mass bias correction on the results of simulations of merging clusters.

Acknowledgements. CAPES, CNPq and UTFPR

References

Albuquerque, R. P., Machado, R. E. G., & Monteiro-Oliveira, R. 2024, MNRAS, 530, 2146
Dehnen W., 1993, MNRAS, 265, 250
Diemer B., Joyce M., 2019, ApJ, 871, L168
Duffy A. R., Schaye J., Kay S. T., Dalla Vecchia C., 2008, MNRAS, 390, 64
Dutton A. A., Macciò A. V., 2014, MNRAS, 441, 3359
Hernquist L., 1990, ApJ, 356, L359
Jing Y. P., 2000, ApJ, 535, L30
Jauzac M. et al., 2018, MNRAS , 481, 2901
Kravtsov A. V., Borgani S., 2012, ARA&A, 50, 353
Kravtsov, A. V. & Borgani, S. 2012, ARA&A, 50, 353
Laganá T. F., Martinet N., Durret F., Lima Neto G. B., Maughan B., Zhang Y. Y., 2013, A&A, 555, 66
Lee W. et al., 2023, ApJ, 945, L71
Molnar, S. M. 2016, Frontiers in Astronomy and Space Sciences, 2, 7

Navarro J. F., Frenk C. S., White S. D. M., 1996, ApJ, 462, L563
Nelson D. et al., 2019, Comput. Astrophys. Cosmol., 6, 2
Pratt G. W., Arnaud M., Biviano A., Eckert D., Ettori S., Nagai D., Okabe N., Reiprich T. H., 2019, Space Sci. Rev., 215, 25
Ruggiero R., Lima Neto G. B., 2017, MNRAS, 468, 4107
Springel V., Pakmor R., Zier O., Reinecke M., 2021, MNRAS, 506, 2871
Wittman D., Stancioli R., Finner K., Bouhrik F., van Weeren R., Botteon A., 2023, ApJ, 954, L36